# The reactions $CH_nD_{4-n}+OH\rightarrow P$ and $CH_4+OD\rightarrow CH_3+HOD$ as a test of current direct dynamics computational methods to determine variational transition-state rate constants. I.

Laura Masgrau, Àngels González-Lafont, and José M. Lluch[a)]
*Departament de Química, Universitat Autònoma de Barcelona, 08193 Bellaterra, Barcelona, Spain*

(Received 12 July 2000; accepted 2 November 2000)

In the present work, we have theoretically calculated the rate constants and their temperature dependence for the reactions $CH_nD_{4-n}+OH\rightarrow P$, and for the reaction of methane with OD, by means of variational transition-state theory plus multidimensional tunneling corrections, at the MP-SAC2//MP2/cc-pVTZ/// and CCSD(T)//MP2/cc-pVTZ/// electronic levels. Also, the newly developed single-point energy interpolation algorithm has been used at the CCSD(T)/aug-cc-pVTZ//MP2/cc-pVTZ and CCSD(T)-SAC//MP2/cc-pVTZ levels. For reactions with $n=1$, 2 or 3, the competitive canonical unified statistical theory has been applied as they involve more than one nonequivalent reaction channel. Variational effects and tunneling have been found to be very important. The proton shift classical energy barrier turns out to be 5.83 and 4.97 kcal/mol at the CCSD(T)/aug-cc-pVTZ//MP2/cc-pVTZ and CCSD(T)-SAC//MP2/cc-pVTZ levels, respectively. Even though we have used the highest *ab initio* electronic level reported up to now for dynamics calculations on these reactions, and although our results are quite good, we still do not match exactly the available experimental data. From our results it can be inferred that, probably, an adiabatic energy maximum between the CCSD(T)-SAC//MP2/cc-pVTZ and CCSD(T)/aug-cc-pVTZ//MP2/cc-pVTZ values (5.6 and 6.2 kcal/mol, respectively, for the perprotio reaction) could be the most feasible, and that the description of the adiabatic profile fails especially in that region away from the transition-state location but crucial for tunneling corrections.  [DOI: 10.1063/1.1335655]

## I. INTRODUCTION

The hydroxyl radical (OH) is widely recognized as the most important oxidant in the earth's troposphere, and is largely responsible for the removal of many of the atmospheric pollutants.[1–4] Thus, understanding of the mechanisms and kinetics of the reactions in which the OH is involved has become a central point in order to model and control the most important atmospheric chemical processes. In turn, methane is one of the most important and most abundant trace organic gases in the atmosphere. By means of the reaction

$$OH+CH_4\rightarrow H_2O+CH_3, \tag{R1}$$

methane controls the abundance of OH in the troposphere. Then, reaction (R1) is essential to build up models to help interpret the chemistry of atmospheric reactions.

For the last three decades the kinetics of reaction (R1) and several H/D isotopic variants have been the object of many of experimental measurements.[5–12] To our knowledge, the most recent results are those reported by Ravishankara and co-workers,[12] who have provided the rate constants for the reactions of OH with methane [reaction (R1)] and each of its deutero-isotopomers, along with the reaction of OD with methane, at different ranges of atmospherically important temperatures (below 422 K)

$$OH+CH_3D\rightarrow H_2O+CH_2D \quad \text{and} \quad HDO+CH_3, \tag{R2}$$

$$OH+CH_2D_2\rightarrow H_2O+CHD_2 \quad \text{and} \quad HDO+CH_2D, \tag{R3}$$

$$OH+CHD_3\rightarrow H_2O+CD_3 \quad \text{and} \quad HDO+CHD_2, \tag{R4}$$

$$OH+CD_4\rightarrow HDO+CD_3, \tag{R5}$$

$$OD+CH_4\rightarrow HDO+CH_3. \tag{R6}$$

Those rate constants were measured using the pulsed photolytic production of OH or OD followed by its detection via pulsed laser induced fluorescence.

On the other hand, for some time reactions (R1) and (R5) have been used as a test for assessing the capability of theoretical chemistry to get accurate values of rate constants of gas-phase reactions (atmospheric or combustion reactions). In this sense, the results of Ravishankara and coworkers now provide an excellent reference in order to discuss the accuracy of the theoretical rate constants found by different methods.

Truong and Truhlar[13] carried out one of the first kinetic studies of reaction (R1) with conventional transition-state theory (TST) and an Eckart model for the calculation of the semiclassical tunneling. The level of electronic structure calculations was second-order Møller–Plesset-scaling all correlation energy,[14] with several basis sets. They predicted rate constants of the same order of magnitude as the experimental data available in that time within the temperature range 200–2000 K.

a)Electronic mail: lluch@klingon.uab.es

 

Later, Melissas and Truhlar[15] used a second-order version of interpolated canonical variational transition state theory[16] (IVTST-2) with multidimensional small-curvature tunneling[17] (SCT) corrections to compute the rate constants for the reactions (R1) and (R5) at a range of temperatures. The level of electronic structure calculations they employed was second-order Møller–Plesset-scaling all correlation energy[14] for the final energy, but optimizing the minimum energy and transition-state structures without scaling, along with an adjusted correlation-consistent polarized-valence triple-zeta basis set, that is, an MP-SAC2//MP2/adj-cc-pVTZ level. Ravishankara and co-workers[12] claim that the calculated values of Melissas and Truhlar are systematically higher than their experimental data, but a careful comparison of both sets of results shows that the agreement is quite good (always within a factor of 2.0) (see also Tully and co-workers).[9] In fact, the theoretical rate constants underestimate the experimental values, except at the lowest temperature range (below 295 K) and at the highest temperatures ($>$1000 K) where they become higher. Melissas and Truhlar have found that tunneling significantly increases the rate constants for reaction (R1), although they admit that it could be overestimated at low temperatures. This fact could explain the crossing between experimental and theoretical results as temperature decreases. On the other hand, the same authors have found that the generalized transition states variationally move towards products as temperature grows, their location depending on the isotopic substitution.

Then, Hu, Liu, and Truhlar[18] repeated the calculation of the rate constants for reactions (R1) and (R5) by using variational transition-state theory with interpolated optimized corrections[18] (VTST-IOC) and a microcanonical optimized multidimensional ($\mu$OMT) tunneling approximation.[19] When the MP-SAC2//MP2/adj-cc-pVTZ information obtained in the previous work was used as the high-level data, and the semiempirical AM1 method with specific reaction parameters[20] (AM1-SRP) was taken as lower electronic level, the rate constants for both (R1) and (R5) were quite similar to the above-mentioned IVTST-2 ones.[15] Since in this case the lower studied temperature was 300 K, the theoretical rate constants are always somewhat smaller than the experimental ones [except at 1500 K for (R1)]. Conversely, when the lower electronic level is the semiempirical PM3 method, the theoretical rate constants become higher than the experimental ones below 350 K and also for (R1) at 1500 K.

On the other hand, Dobbs, Dixon, and Komornicki[21] have studied reaction (R1) using conventional transition-state theory and the Wigner correction to account for tunneling. The electronic level was the unrestricted second-order Møller–Plesset method, with a triple-zeta basis set augmented by two sets of polarization functions and a set of $f$ functions on C and O atoms (UMP2/TZ+2P+$f$) for geometries and frequencies; and the quadratic configuration interaction using single and double substitutions with a triples correction, with a Dunning's correlation-consistent basis set for C and O atoms augmented by a set of diffuse $s$ and $p$ functions and his correlation-consistent basis set for H [QCISD(T)/CC] for the calculation of energies. The corresponding rate constants turn out to be higher than the experimental values of Ravishankara and co-workers[8,12] and the theoretical values of Melissas and Truhlar[15a] above 250 K, although they become quite close to the experimental results at lower temperatures (200 K).

Very recently, two more additional computational studies of the kinetics of hydrogen abstraction by the OH radical from methane and its fluoroderivatives ($CH_3F$, $CH_2F_2$, $CHF_3$) have been published with the main purpose of finding the most adequate theoretical methodology to calculate that kind of hydrogen abstraction rate constant. In the first work, Schwartz *et al.*[22] use conventional transition-state theory to study the hydrogen abstraction reaction from methane in the temperature range from 250–2000 K. Tunneling is included using a monodimensional Eckart potential energy function. Schwartz *et al.* obtain the imaginary frequency that is needed in the calculation of the Eckart transmission coefficient, at the maximum of the Eckart function from a fit to single-point G2 energies along the MP2/6-31G($d$) minimum energy path (MEP). The fitted imaginary frequency of 1165 $cm^{-1}$ is much lower than the HF/6-31G($d$) frequency of 2836 $cm^{-1}$ and 60% lower when compared to the QCISD/6-311G frequency of 1885 $cm^{-1}$. This result corresponds to a much broadcr MEP at the G2//MP2/6-31G($d$) level. The authors calculate the tunneling coefficients for an Eckart function fitted to the adiabatic energies [classical energy plus vibrational zero-point energy (ZPE)] at reactants, products, and saddle point by readjusting slightly the imaginary frequency at the maximum of the Eckart profile. This adjustment lowers the barrier and results in a somewhat more diminished imaginary frequency (1084 $cm^{-1}$). Consequently, the Eckart tunneling efficiencies are drastically reduced compared with the initial ones that were calculated using the HF/6-31G($d$) frequency. However, the TST rate constants with the new fitted adiabatic Eckart profile become systematically too low in comparison to experimental results. To improve accuracy, the classical barrier height was finally adjusted to require that $k_{TST}=k_{exp}$ at 298 K and these final adjusted rate constants show, in general, a very good agreement with experimental results for which measured rates are available. The authors conclude that fitting the high-level potential energy surface (PES) is the only currently feasible procedure for calculating accurate tunneling factors because incorrect values of the reaction path imaginary frequency constitute the greatest source of error in the calculation of the tunneling factors for hydrogen atom abstraction reactions.

Finally, Korchowiec *et al.*[23] have published another study on the hydrogen abstraction reaction from methane and hydrofluoromethanes by the OH radical. The rate constants are calculated in the temperature range 280–420 K according to the conventional transition-state theory and tunneling is neglected or included with the Wigner correction formula assuming no significant curvature on the Arrhenius plots for the four reactions. The reaction enthalpies and the activation energies are calculated using several G2 type schemes. The authors conclude that the G2M scheme (where the geometries and ZPEs are calculated at the B3LYP/6-311G($d,p$) level) gives accurate reaction enthalpies and the influence of fluorine substitution is correctly described qualitatively. In particular, for the hydrogen abstraction reaction from meth-

ane, the reaction enthalpy at 298 K deviates only from experiment by 0.2 kcal/mol. For the activation energies, the values calculated with the G2M barrier heights using the Wigner tunneling correction show the best agreement with experimental results although, even in this case, the activation energies were slightly overestimated. The influence of fluorine substitution on the activation energies was also qualitatively reproduced using the G2M PES and the TST/Wigner rate constant calculations. Consequently, Korchowiec *et al.*[23] conclude that the G2M scheme works well for this kind of hydrogen abstraction reactions in gas phase.

At this point, it could seem that for the study of the dynamics of reactions of OH with methane and each of its deutero-isotopomers, the best methodology consists of calculating TST rate constants based on high-level electronic energies (using G2-type schemes) at selected points on the PES followed by the correction for tunneling effects based on the monodimensional Eckart formula or the Wigner expression (in both cases using low imaginary frequencies at the saddle point $\sim 1000\ \mathrm{cm}^{-1}$). However, when compared to experiment, the results of Schwartz *et al.*[22] and Korchowiec *et al.*[23] are not clearly better than the rate constants calculated by Truhlar and co-workers.[15,18] In fact, the rate constants and activation energies obtained by Truhlar and co-workers with IVTST-2 and VTST-IOC methodologies are closer to experiment than the results of the ''revised procedure'' (before the final adjustment) by Schwartz *et al.* and better than the TST/Wigner activation energies of Korchowiec *et al.* in the temperature range 280–420 K.

On the other hand, very recently analytical PES for the title reactions have been fitted by Espinosa-García and Corchado[24] to reproduce the experimental thermal rate constants and kinetic isotope effects, along with the saddle point properties corresponding to the already available *ab initio* calculations. Although no new electronic structure calculations have been carried out by these authors, their work provides analytical PES that can be used for trajectory calculations. Interestingly, their dynamical calculations show noticeable variational effects.

The aim of the present work is to show by means of new electronic structure calculations at higher level and newly developed schemes of variational transition-state theory with multidimensional tunneling corrections[25,26] (VTST/MT) that, in agreement with the studies of Truhlar and co-workers[15,18] and Espinosa-García and Corchado,[24] variational effects and multidimensional tunneling effects must be accounted for in the dynamics study of (R1) to (R6) protium/deuterium abstraction reactions. In this respect, this work represents a methodological continuation to the studies of Truhlar and co-workers and it is also the application of VTST/MT methodologies to a larger number of isotopically substituted hydrogen abstraction reactions. The comparison to the experimental rate coefficients for (R1) to (R6) will serve as a very difficult test for the ability of direct dynamics theoretical methods to compute rate constants (that is, without using any global or semiglobal analytical PES).

## II. METHOD OF CALCULATION

In this section we will first focus on the perprotio reaction and later we will comment on the isotopically substituted abstraction processes.

The GAUSSIAN 94[27] system of programs was used for all the electronic structure calculations and the direct dynamics VTST/MT calculations were carried out with the POLYRATE 8.2[28] code.

### A. Perprotio reaction

Stationary point geometries, first and second derivatives were calculated at second-order Møller–Plesset perturbation theory[29,30] (MP2) based on restricted Hartree–Fock (RHF) or unrestricted Hartree–Fock[29] (UHF) wave functions for closed-shell and open-shell systems, respectively. The basis set is a correlation-consistent polarized-valence triple-zeta[31] (cc-pVTZ) of Dunning with pure *d* and *f* functions. Furthermore, we have carried out single-point energy calculations at those geometries using the coupled-cluster method, including single and double excitations and a perturbative estimate of the effect of triple excitations,[32] with the same basis set [CCSD(T)/cc-pVTZ], and CCSD(T) calculations using the augmented correlation consistent basis set of Dunning[33,34] [CCSD(T)/aug-cc-pVTZ]. We have also done single-point energy calculations at MP2/cc-pVTZ geometries using one of the general parametrizations of the SAC (scaling-all-correlation) method for semiempirical extrapolation of electronic structure calculations recently published by Truhlar *et al.*[35] In particular, we have used the CCSD(T)-SAC/cc-pVTZ scheme with a scaling factor equal to 0.8928. A full electron correlation treatment was employed both at MP2 and at CCSD(T) correlation levels. For the sake of comparison with the previous calculations of Truhlar and co-workers,[15,18] results at MP2/adj-cc-pVTZ and at MP-SAC2//MP2/adj-cc-pVTZ are also presented.

We have calculated the minimum energy path[36] at MP2/cc-pVTZ level by following the Gonzalez–Schlegel mass-weighted internal coordinates reaction path algorithm.[37] We have used a gradient step size, $\delta s$, of 0.005 29 Å (where $s$ denotes the distance along the MEP in an isoinertial mass-weighted coordinate system[38,39] with a scaling mass equal to 1 amu) to follow the MEP downhill enough to ensure convergence in the tunneling calculations. Geometries, energies, gradients, and Hessians of 35 nonstationary points along this MEP, from $s=-2.20$ bohr to $s=0.50$ bohr (with $s=0$ at the saddle point, $s$ negative on the reactant side of the saddle point, and positive on the product side), have been used in the dynamical calculations as a low level, as will be explained later. We have employed canonical variational transition-state theory[38–43] (CVT) plus multidimensional tunneling (MT) contributions for calculating the rate constants over a wide range of temperatures. The small-curvature tunneling[17] (SCT) semiclassical adiabatic ground-state approximation has been used to correct for tunneling. The CVT/SCT rate constant is given by

$$k^{\mathrm{CVT/SCT}}(T,s_*) = \kappa^{\mathrm{SCT}}(T)\frac{\sigma k_B T}{h}\frac{Q^{GT}(T,s_*)}{Q^R(T)}\exp(-V_{\mathrm{MEP}}(s_*)/k_B T), \quad (1)$$

where $\kappa^{\mathrm{SCT}}(T)$ is the SCT transmission coefficient, $s_*$ denotes the value of $s$ at the free energy maximum along the MEP at temperature $T$, $\sigma$ is the symmetry factor,[44] $k_B$ is Boltzmann's constant, $h$ is Planck's constant, $Q^R(T)$ is the reactants partition function per unit volume excluding symmetry numbers for rotation, $Q^{GT}(T,s_*)$ is the partition function of the generalized transition state at $s_*$ excluding again symmetry numbers for rotation, and $V_{\mathrm{MEP}}(s_*)$ is the classical potential energy at $s_*$.

We have applied the reoriented dividing surface[45] (RODS) algorithm in order to improve the generalized frequencies along the MEP. The normal mode analysis has been performed in redundant internal coordinates[46] (six stretches, eight bends, and four torsions). All vibrations have been treated within the harmonic approximation (with a scale factor of 0.9790)[35,47] except the internal rotational motion corresponding to the lowest mode at the saddle point and along the MEP. For this mode we have used the hindered rotor approximation of Truhlar and co-workers[48] for calculating the partition function. In particular, we have used the scheme denoted as CW. In this scheme one obtains the data required to specify the torsional potential as follows: the moment of inertia for internal rotation at all stationary points structures and at each geometry along the MEP is calculated using Kilpatrick and Pitzer's protocol;[49] the classical potential energy barrier for the internal rotational motion is obtained from electronic structure calculations at the saddle point or from experiment and the harmonic frequency is then calculated from those two parameters (moment of inertia and rotational barrier). Our calculation gives a curvilinear moment of inertia equal to $1.48\times10^{-47}\,\mathrm{kgm}^2$ (5800 a.u.) at the saddle point with the assumption that the two subsystems rotating with respect to each other are OH and $HCH_3$. The classical potential energy barrier for the internal rotation is equal to 0.006 kcal/mol at the MP2/cc-pVTZ level of theory and the harmonic frequency given by the CW scheme at the saddle point (18 $\mathrm{cm}^{-1}$) is in good agreement with the one obtained from the MP2/cc-pVTZ electronic structure calculation (21 $\mathrm{cm}^{-1}$). The symmetry number for the internal rotation has been taken as 3.

For the electronic partition functions we have assumed no low-lying excited state of the $^2A_1$ saddle point, but we have included the $^2\Pi_{1/2}$ excited state (140 $\mathrm{cm}^{-1}$) of OH in the reactant partition function.

We have applied two different kinds of dual level direct dynamics schemes. For both of them we have used the same low level (LL): MP2/cc-pVTZ. The high-level (HL) calculations have only been used to correct the energy. In the first method we have calculated the single-point CCSD(T)/cc-pVTZ//MP2/cc-pVTZ/// high level energy at all 35 nonstationary geometries along the low level MEP (the X//Y/// notation indicates single-point energy calculations at level X that are performed along the path calculated at level Y, not just at the stationary points). This high-level energy has been interpolated by the mapping procedure[50] in order to obtain $V_{\mathrm{MEP}}^{\mathrm{HL}}(s)$, that is, the HL classical potential energy profile. The second dual level methodology that we have used (denoted here as HL//LL) is a version of the interpolation single-point energy correction scheme,[51] which uses a mapping function[51b] to interpolate the energy difference of a few single-point high-level energies from the corresponding low-level ones (ISPE). The low-level energy is corrected in order to approximate $V_{\mathrm{MEP}}^{\mathrm{HL}}(s)$. The ISPE method can be applied for a minimum of three high-level points (reactants, saddle point, and products). We have used those three stationary points plus single-point energy calculations at five nonstationary points along the MEP to carry out ISPE calculations at the CCSD(T)/cc-pVTZ//MP2/cc-pVTZ, CCSD(T)/aug-cc-pVTZ//MP2/cc-pVTZ, and CCSD(T)-SAC//MP2/cc-pVTZ levels of theory.

In order to compare the methodology employed in the present work with previous works on this reaction by Truhlar *et al.*,[15,18] we have also made a dual level direct dynamics calculation following the first single-point energy approach; that is, calculating HL single-point energies all along the MEP, at the MP-SAC2//MP2/adj-cc-pVTZ/// level of theory.

### B. Isotopically substituted reactions

The general methodology we have used for the isotopically substituted reactions is the same as the one we have employed for the perprotio reaction, but some changes had to be included. By definition, the MEP depends on the atomic masses of the atoms involved in the reaction and, therefore, for each isotopic substitution a new MEP should be calculated. Applying the RODS algorithm allows us to use the perprotio MEP as the reaction path for the isotopically substituted reactions. Thus, although we didn't calculate the MEP for each reaction (R2)–(R6), using the RODS algorithm we obtain reliable generalized eigenvectors and frequencies, and we can calculate the vibrationally adiabatic ground-state potential energy curve[25,36a,39–41] for each isotopic substitution as

$$V_a^G(s) = V_{RP,M}(s) + \varepsilon_{\mathrm{tran}}^G(s), \quad (2)$$

where $s$ is again the distance along the reaction path in an isoinertial mass-weighted coordinate system with the scaling mass equal to 1 amu (so, given a geometry, $s$ changes with the isotopic substitution), $V_{RP,M}(s)$ is the minimum classical potential energy in the reoriented dividing surface at $s$ on the reaction path (which we took as the perprotio MEP), and $\varepsilon_{\mathrm{tran}}^G(s)$ is the zero-point energy (ZPE) at $s$ from the generalized normal-mode vibrations transverse to the reaction path.

Actually, if we take a look at reactions (R2)–(R6) we can see that (R2), (R3), and (R4) involve more than one vibrationally adiabatic ground-state potential energy profile. For each of these reactions we have that the given reactants can react via different channels yielding two pairs of isotopically nonequivalent products. Depending on the position of the deuterium atom(s) in the molecule we obtain different values of $s$, frequencies [that is, $\epsilon_{\mathrm{tran}}^G(s)$], and $V_{RP,M}(s)$.

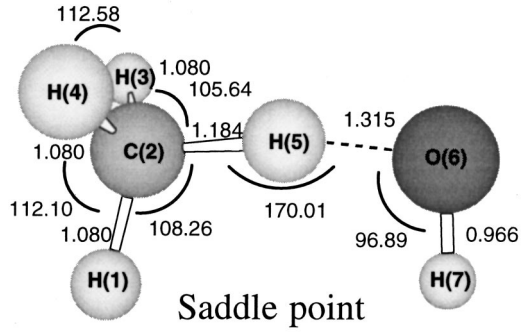


FIG. 1. Optimized saddle point geometry (distances in angstroms and angles in degrees) at the MP2/cc-pVTZ level.

Thus, there are different $V_a^G(s)$ and different free-energy profiles as a function of temperature. In this situation of parallel channels we have to apply the competitive canonical unified statistical theory[52] (CCUS), and the final reaction rate constant, $k(T)$, is given by

$$k(T)=\sum_i k_i(T), \tag{3}$$

where $i$ is the number of isotopically nonequivalent channels and $k_i(T)$ is the CVT/SCT rate constant calculated for each of these channels.

## III. RESULTS AND DISCUSSION

In this section, the results corresponding to the electronic structure calculations on the $CH_4+OH\rightarrow CH_3+H_2O$ reaction are first presented. The dynamical results for the perprotio reaction and the isotopically substituted reactions will be described later.

### A. Electronic structure calculations

The optimized structures for the reactants ($CH_4$ and OH) and products ($CH_3$ and $H_2O$) at the MP2/cc-pVTZ level are given in Table I of Ref. 15a. The saddle point geometric structure at the MP2/cc-pVTZ level is depicted in Fig. 1. The C(2)···H(5) (1.184 Å) distance is shorter than the H(5)···O(6) distance (1.315 Å), in agreement with the early transition state expected for an exothermic reaction. The H(5)···O(6)–H(7) angle is almost perpendicular to the C(2)···O(6) axis and the O(6)–H(7) bond is eclipsed with a methyl group C(2)–H(1) bond (H(1)–C(2)···O(6)–H(7) dihedral angle of 0.0°) in agreement with previous calculations.[15a,21,22,53] The staggered conformer is a second-order saddle point which corresponds to the local maximum along the internal relative rotation motion of the methyl group around the reactive H(5)···O(6) bond at the saddle point structure. The bond lengths and bond angles of the second-order transition state are not significantly different from those of the first-order structure. The transition state eigenvector corresponding to the imaginary frequency is primarily a motion of the hydrogen atom transferring between the C(2) and O(6) centers. The magnitude of the scaled transition-state imaginary frequency of 1746 $cm^{-1}$ is 1.63 times smaller than the scaled HF/6-31G($d$) frequency (of 2836 $cm^{-1}$) used in the G2 method[22] but 1.61 times higher than the final adjusted Eckart frequency of 1084 $cm^{-1}$ of Schwartz *et al.*[22] The MP2/cc-pVTZ imaginary frequency differs from the MP2/adj-cc-pVTZ imaginary frequency by 78 $cm^{-1}$ and both values are quite similar to the QCISD/6-311G imaginary frequency (1885 $cm^{-1}$) calculated by Schwartz *et al.* For the second-order saddle point the larger imaginary frequency corresponds to the motion of the H(5) atom transferring between the C(2) and O(6) centers, whereas the eigenvector for the smaller one corresponds to the relative motion of the methyl group around the reactive H(5)···O(6) bond. Beginning from the eclipsed MP2/cc-pVTZ saddle point the MEP was calculated for the perprotio reaction in order to obtain the necessary information of the PES for the dynamical study of (R1) to (R6) reactions.

Table I summarizes the results for the energetics of the stationary points of the (R1) reaction. These energy values indicate, in agreement with previous calculations,[53] that the perprotio reaction pathway at 0 K presents in the exit channel a van der Waals well on the MP2/cc-pVTZ PES that, following the MEP, connects with the saddle point. This complex presents a $H_3C\cdots H-OH$ configuration and it is bound in our calculations at 0 K and higher temperatures. The product complex geometry is presented in Fig. 2. Basch *et al.*[53] have also found a reactant complex with the ''unexpected'' $H_4C\cdots H-O$ interaction and a classical binding energy of 0.9 kcal/mol at the UMP2/6-311++G($2d,p$) level. They indicate that this complex is not on the MEP for the perprotio reaction and that the complex is calculated to be unbound at room temperature. This stationary structure has also been located very recently by Wheeler *et al.*[54] Likewise, we have found this minimum on the MP2/cc-pVTZ PES away from the hydrogen abstraction MEP. In any case, due to the location of the reactant and product complexes on the

TABLE I. Energies (kcal/mol) of the stationary points for the $CH_4+OH\rightarrow CH_3+H_2O$ reaction. $V_{PC}$ is the classical energy of the product complex; $(\Delta V_a^G)_{PC}$ is the adiabatic depth of the product complex; $V^{\neq}$ is the classical energy barrier; $\Delta V_a^{G\neq}$ is the adiabatic energy barrier; $\Delta V$ is the classical reaction energy.

| Method | $V_{PC}$ | $(\Delta V_a^G)_{PC}$ | $V^{\neq}$ | $\Delta V_a^{G\neq}$ | $\Delta V$ |
|---|---|---|---|---|---|
| MP2/cc-pVTZ[a] | −16.87 | −17.10 | 8.38 | 7.01 | −14.96 |
| MP2/adj-cc-pVTZ | ··· | ··· | 7.96 | 6.48 | −12.86 |
| CCSD(T)//MP2/cc-pVTZ[a] | −12.82 | −13.05 | 7.08 | 5.71 | −10.90 |
| MP-SAC2//MP2/adj-cc-pVTZ | ··· | ··· | 7.36 | 5.88 | −13.27 |
| CCSD(T)/aug-cc-pVTZ//MP2/cc-pVTZ[a] | −14.48 | −14.70 | 5.83 | 4.46 | −12.46 |
| CCSD(T)-SAC//MP2/cc-pVTZ[a] | −14.18 | −14.42 | 4.97 | 3.60 | −12.07 |

[a]All frequencies are scaled by 0.9790.

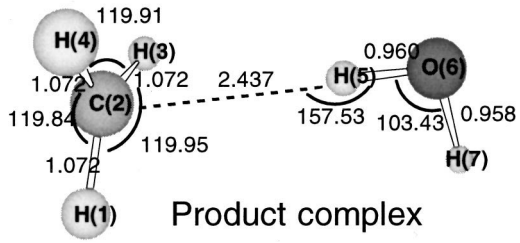


FIG. 2. Optimized product complex geometry (distances in angstroms and angles in degrees) at the MP2/cc-pVTZ level.

potential energy surface and to the proton shift energy barrier, the kinetic reaction pathway for the perprotio reaction can be thought to take place at 0 K and at higher temperatures through only one dynamical bottleneck corresponding to that hydrogen abstraction process.[55]

The best result for the classical reaction energy of the perprotio reaction given in Table I corresponds to the MP-SAC2 method of Truhlar and co-workers.[15a] It has to be pointed out, though, that the scaling factor in the MP-SAC2 scheme was chosen to make the calculated classical reaction energy agree perfectly well with the experimental value of $-13.27$ kcal/mol (a slightly different value for the experimental classical reaction energy of $-13.47$ kcal/mol has also been employed by Truhlar and co-workers[56] more recently). The results in the literature[21,23,57] have shown that the hydrogen abstraction reaction exoergicities calculated with the MP2 methods are closer to the experimental values than those calculated with the MP4, QCISD(T), and CCSD(T) methods when using small to medium basis sets. However, increasing the basis set tends to increase the exoergicity and at the MP2/cc-pVTZ level (Table I) the reaction classical energy is already $-1.5$ kcal/mol off. Electronic structure calculations at the CCSD(T) level have a tendency to underestimate reaction energies of hydrogen abstraction processes as compared with experiment and this may result from the slow convergence of the calculations with the dimensions of the basis sets.[35,58] Using then the more systematic correlation-consistent basis set, we have obtained that at the CCSD(T)//MP2/cc-pVTZ level there is a difference of 2.57 kcal/mol compared with the experimental exoergicity. This energy difference decreases to 1.40 kcal/mol with the SAC extrapolation at the CCSD(T)-SAC//MP2/cc-pVTZ level and to 1.01 kcal/mol increasing the basis set at the CCSD(T)/aug-cc-pVTZ//MP2/cc-pVTZ level. The exothermicity of the $CH_4+OH\rightarrow CH_3+H_2O$ reaction at 298 K can be estimated using heats of formation or hydrogen atom bond dissociation energies to give $-14.5$ and $-14.8$ kcal/mol, respectively.[53] The calculated exothermicity at 298 K at the CCSD(T)/aug-cc-pVTZ//MP2/cc-pVTZ level and at the CCSD(T)-SAC//MP2/cc-pVTZ level are $-13.6$ kcal/mol and $-13.2$ kcal/mol, respectively. Those two values show a good agreement with the exothermicity at the CBS/QCI-APNO level ($-13.5$ kcal/mol) of Malick *et al.*[59] In any case, the best published values for the $CH_4+OH\rightarrow CH_3+H_2O$ reaction enthalpy at 298 K are given by the G2MP2 ($-14.1$ kcal/mol) and the G2M ($-14.2$ kcal/mol) methodologies calculated by Korchowiec *et al.*[23]

From the values of the classical potential energy barriers in Table I, it can be inferred that they are also very dependent on the level of calculation and the basis set, as it has already been observed in previous works.[21–23,53,57] At the CCSD(T) level the classical potential energy barriers are lower than the MP2 or MP-SAC2 barriers. The classical potential barrier height decreases 1.25 kcal/mol when at the CCSD(T) level the correlated basis set is improved by adding diffuse functions. The classical potential energy barrier decreases even more (around 0.86 kcal/mol) when using the SAC scheme. At present there is a bench of electronic structure results of the classical potential energy barrier for the $CH_4+OH\rightarrow CH_3+H_2O$ reaction. The classical potential energy barrier in the G2M scheme, which gives the most accurate reaction enthalpy, is 5.3 kcal/mol whereas the barrier at the G2//MP2/6-31G($d$) level is 7.45 kcal/mol.[23] The calculation of the classical potential energy barrier for the perprotio reaction is 5.11 kcal/mol at the CBS/QCI/APNO level[59] (corrected by $-0.15$ kcal/mol to account for spin–orbit effects) which agrees with our value of 4.97 kcal/mol at the CCSD(T)-SAC//MP2/cc-pVTZ level. The CCSD(T) calculation previously[53] done on this reaction gives a barrier of 8.6 kcal/mol at the CCSD(T)//MP2/6-311++G($2d,p$) level, much higher than our coupled-cluster method results. DFT methods give very low barriers[53,56,60–62] (2.58 kcal/mol with B3LYP/TZ2P method for the perprotio reaction)[60] but those results were proven to be in error because DFT methods fail to describe hydrogen abstraction reactions because of the creation of an apparent ''extra bond'' at the transition state.

In view of such a dispersion of electronic structure results on the perprotio reaction, we agree with a recent assessment of Truhlar and co-workers[63] pointing out that one of the main difficulties in calculating reliable rate constants by reaction-path methods is the effectiveness of electronic structure calculations to properly characterize the stationary points. Then, it seems that the best way to estimate the actual barrier height is to carry out full dynamical calculations of the rate constant for realistic potential energy surfaces and compare this calculation to experiment. However, when variational effects are involved, conventional transition-state theory should not be used. Moreover, when tunneling is important a monodimensional approach might not be accurate enough. Then, the properties of the PES that are crucial for the rate constant results are not only the barrier height at the saddle point, but also the location of the variational transition state as a function of temperature, the width of the energy profile, and the swath region. Thus, the effectiveness of electronic structure calculations has to be tested not only at the stationary points, but also along the reaction path (energy and frequencies).

In the following section we present the comparison between experimental rate constants and the dynamical calculations performed in this work for the perprotio reaction and the labeled isotopically reactions. The comparison will then be used to infer the goodness of the calculated potential energy surfaces and the validity of the employed VTST/MT direct dynamics methods.

### B. Dynamical calculations

As indicated in the Introduction, the six reactions are labeled (R1) to (R6). For reaction (R2) [as well as for reaction (R3) and (R4)], the same pair of reactants can give two different pairs of products depending on whether a protium or a deuterium atom is abstracted by the hydroxyl radical. In the calculation of the global reaction rate from a given pair of reactants for (R2) to (R4), those two exit channels constitute competitive processes and their contribution must be added in accordance with CCUS theory. If we define the rate constant for each one of those nine isotopically nonequivalent channels as $k_R(L)$, where R stands for the reactant side numbering and L is the H or D abstracted, the kinetic scheme for the whole set of abstraction reactions can be written in the following form:

$$\begin{aligned} k_1 &= k_1(\mathrm{H}), \\ k_2 &= k_2(\mathrm{H}) + k_2(\mathrm{D}), \\ k_3 &= k_3(\mathrm{H}) + k_3(\mathrm{D}), \\ k_4 &= k_4(\mathrm{H}) + k_4(\mathrm{D}), \\ k_5 &= k_5(\mathrm{D}), \\ k_6 &= k_6(\mathrm{H}). \end{aligned} \tag{4}$$

However, if we now take into account the number of elementary reaction events, each one of those six global abstraction rates can be written as an addition of 12 elementary reaction rates. We can define the rate constants for those individual events on a per hydrogen-atom basis (without symmetry numbers) as: $k_{R,X}(L)$, where R stands again for the reactant side numbering, L is again the H or D abstracted, and X stands for the isotope (H or D) eclipsed to the hydroxyl protium/deuterium at the saddle point structure. The symmetry numbers for each one of the elementary processes are calculated according to the expression[44]

$$\sigma(s) = \frac{n\sigma^R}{\sigma^{GT}(s)}, \tag{5}$$

where $n$ stands for the number of kinetically equivalent transition states, $\sigma^R$ is the usual rotational symmetry number for the reactants (or the product of these symmetry numbers if there are two molecular reactants, as in the present case) and $\sigma^{GT}(s)$ corresponds to the usual rotational symmetry number of the generalized transition state at s. In our applications, $\sigma^{GT}$ is independent of $s$, and thus $\sigma(s)$ becomes a constant $\sigma$. The values for the different variables in Eq. (5) are given in Table II.

With the notation introduced above, we have

$$\begin{aligned} k_1 &= 12 \cdot k_{1,\mathrm{H}}(\mathrm{H}), \\ k_2 &= 6 \cdot k_{2,\mathrm{H}}(\mathrm{H}) + 3 \cdot k_{2,\mathrm{D}}(\mathrm{H}) + 3 \cdot k_{2,\mathrm{H}}(\mathrm{D}), \\ k_3 &= 2 \cdot k_{3,\mathrm{H}}(\mathrm{H}) + 4 \cdot k_{3,\mathrm{D}}(\mathrm{H}) + 4 \cdot k_{3,\mathrm{H}}(\mathrm{D}) + 2 \cdot k_{3,\mathrm{D}}(\mathrm{D}), \\ k_4 &= 3 \cdot k_{4,\mathrm{H}}(\mathrm{D}) + 6 \cdot k_{4,\mathrm{D}}(\mathrm{D}) + 3 \cdot k_{4,\mathrm{D}}(\mathrm{H}), \\ k_5 &= 12 \cdot k_{5,\mathrm{D}}(\mathrm{D}), \\ k_6 &= 12 \cdot k_{6,\mathrm{H}}(\mathrm{H}). \end{aligned} \tag{6}$$

TABLE II. Parameters used to calculate the symmetry numbers according to Eq. (5). See Sec. III.

| Reaction | $n$ | $\sigma^R$ | $\sigma^{GT}$ | $\sigma$ |
|---|---|---|---|---|
| $R_{1,H}(H)$ | 1 | 12 | 1 | 12 |
| $R_{2,H}(H)$ | 2 | 3 | 1 | 6 |
| $R_{2,D}(H)$ | 1 | 3 | 1 | 3 |
| $R_{2,H}(D)$ | 1 | 3 | 1 | 3 |
| $R_{3,H}(H)$ | 1 | 2 | 1 | 2 |
| $R_{3,D}(H)$ | 2 | 2 | 1 | 4 |
| $R_{3,H}(D)$ | 2 | 2 | 1 | 4 |
| $R_{3,D}(D)$ | 1 | 2 | 1 | 2 |
| $R_{4,H}(D)$ | 1 | 3 | 1 | 3 |
| $R_{4,D}(D)$ | 2 | 3 | 1 | 6 |
| $R_{4,D}(H)$ | 1 | 3 | 1 | 3 |
| $R_{5,D}(D)$ | 1 | 12 | 1 | 12 |
| $R_{6,H}(H)$ | 1 | 12 | 1 | 12 |

We see that, for instance, the global rate constant $k_1$ accounts for the scission of a C–H bond by 12 equivalent kinetic pathways. In turn, $k_2$ accounts for the scission of a C–H bond by 9 kinetic pathways (which can be classified in two groups of 6 and 3 equivalent kinetic pathways, respectively) and $k_2$ also accounts for the scission of a C–D bond by 3 equivalent kinetic pathways. In going from (R1) to (R5), the contribution of C–D bond breaking to the global rate constant increases.

The 13 individual elementary rate constants $k_{R,X}(L)$ have been calculated using direct VTST/MT reaction path dynamics. As explained in Sec. II, two different dual-level approaches of the type HL//LL/// and HL//LL, respectively, have been used. In those approaches, which can be called ''single-point energy approaches,'' one first calculates the reaction path at the lower level but then corrects the energy along the reaction path without reoptimizing any geometries.

We first present results with single-point HL energies calculated for the whole set of LL geometries along the path. The HL energy is interpolated by means of a mapping procedure. In Table III the calculated rate constants ($k_1$ for R1) at the MP-SAC2//MP2/adj-ccpVTZ/// level and at the CCSD(T)//MP2/cc-pVTZ/// level are compared to experimental results in the temperature range 200–1500 K. One can observe that the two dual-level dynamical calculations underestimate the experimental rate constants especially in the low temperature range. However, the SAC correction at the MP2 level better approaches the experimental results.

The MP-SAC2//MP2-adj-cc-pVTZ/// calculation has also been included to compare with previous calculations of Truhlar and co-workers[15a,18] where they were using the same high level. In fact, the IVTST-2 and VTST-IOC rate constants of Truhlar and co-workers are direct dynamics approaches trying to reproduce the MP-SAC2//MP2/adj-cc-pVTZ/// rate constants. However, our MP-SAC2 CVT/SCT rate constants are lower than the ones of Truhlar and co-workers (a factor of 0.03 at 223 K when compared to IVTST-2 rate constant, a factor of 0.14 at 300 K when compared with the VTST-IOC calculation at the AM1-SRP-IOC level, and a factor around 0.65 at 1500 K in comparison with the two previous dynamical calculations). These significant differences may come from the failure of interpolated VTST

TABLE III. Rate constants (in $cm^3\,molecule^{-1}\,s^{-1}$) at several temperatures (power of 10 in parentheses) for (R1) using three dual-level reaction path dynamics methods, and corresponding experimental values.

| | $k_1^{CVT/SCT}$ | | | |
|---|---|---|---|---|
| $T$(K) | MP-SAC2// MP2/adj-cc-pVTZ/// | CCSD(T)// MP2/cc-pVTZ/// | VTST-ISPE[a] | $k_1^{exp}$ |
| 200 | 2.04(−17) | 6.90(−18) | 7.16(−18) | 4.0(−16)[b] |
| 223 | 5.51(−17) | 2.23(−17) | 2.28(−17) | 8.2(−16)[b] |
| 298 | 6.88(−16) | 3.75(−16) | 3.77(−16) | 6.35(−15)[c] |
| 300 | 7.27(−16) | 3.98(−16) | 4.00(−16) | 6.62(−15)[c] |
| 350 | 2.43(−15) | 1.47(−15) | 1.47(−15) | 1.63(−14)[c] |
| 400 | 6.40(−15) | 4.11(−15) | 4.11(−15) | 3.38(−14)[c] |
| 420 | 8.96(−15) | 5.86(−15) | 5.86(−15) | 4.37(−14)[c] |
| 500 | 2.76(−14) | 1.91(−14) | 1.91(−14) | 1.34(−13)[d] |
| 600 | 8.03(−14) | 5.77(−14) | 5.77(−14) | 2.95(−13)[d] |
| 700 | 1.83(−13) | 1.35(−13) | 1.35(−13) | ··· |
| 1000 | 9.92(−13) | 6.98(−13) | 6.97(−13) | 1.93(−12)[d] |
| 1500 | 5.06(−12) | 3.65(−12) | 3.65(−12) | 6.65(−12)[d] |

[a]CCSD(T)//MP2/cc-pVTZ.
[b]From Ref. 12.
[c]From Ref. 8.
[d]From Ref. 7.

methodologies to reproduce HL results or from differences in the way the calculations were done. In our dual-level MP-SAC2//MP2/adj-cc-pVTZ/// calculation the highest energy point along the lower level path, that is, max ($V^{HL//LL}$), has been shifted to the saddle point position in accordance with the IVTST-2 and IVTST-IOC methodologies, but the MP-SAC2//MP2/adj-cc-pVTZ/// classical potential energy profile is wider than the ones interpolated by those two previous VTST/MT calculations. In addition, the MP2-SAC2//MP2/adj-cc-pVTZ/// adiabatic curve is higher and wider than the IVTST-2 and the VTST-IOC adiabatic profiles. In the three direct dynamics calculations, the frequencies are harmonic except for the lowest vibrational mode that has been described by a hindered partition function. Moreover, for the MP2-SAC2//MP2/adj-cc-VTZ/// dual-level calculation we have also adopted the reduced moment of inertia of 7690 a.u. calculated by Truhlar and co-workers with a rectilinear algorithm in the two previous studies. Therefore, the differences in the adiabatic curve may come in part from the use of RODS algorithm in our work and even more from the use of redundant internal coordinates instead of Cartesian coordinates to perform generalized normal mode analyses. The generalized normal mode frequencies are not invariant under coordinate transformations at nonstationary points along the reaction path. As a consequence, calculated rate constants depend on the particular choice of the coordinate system. However, the vibrational frequencies obtained with curvilinear coordinates have been found to be more physical than rectilinear vibrational coordinates. Rectilinear coordinates will generally give rise to a lower and thinner adiabatic profile and to higher rates, but rectilinear vibrational frequencies may be unphysical in magnitude or even imaginary over a wide range of the reaction coordinate.[46] Consequently, we have adopted the curvilinear vibrational analysis in our dual-level schemes even though the IVTST-2 and VTST-IOC approaches in Cartesian coordinates give much better rate constants when compared to experimental results.

In view of the poor results obtained for the rate constants at the CCSD(T)//MP2/cc-pVTZ/// level, we decided to raise the level of electronic structure calculations by correcting the energies along the path at the CCSD(T)/aug-cc-pVTZ level. However, the calculation of 35 single-point energies along the path at the CCSD(T)/aug-cc-pVTZ//MP2/cc-pVTZ/// level results to be excessively time consuming. For that reason we decided to change our single-point energy approach by the mapped interpolation scheme called VTST-ISPE. The VTST-ISPE methodology has been shown to recover essentially the full advantage of single-point energy corrections from a very small set of such corrections. As indicated above, in the VTST-ISPE scheme one interpolates the energy difference of a few single-point energies along the reaction path between the higher-level HL with the geometries obtained at the low-level LL and the energy from lower-level LL. In order to select the nonstationary points along the reaction path at which single-point energies are calculated, we carried out a systematic comparison between the dual-level direct dynamics results presented in Table III at the CCSD(T)//MP2/cc-pVTZ level based on a dense set of 35 nonstationary points and the CVT/SCT rate constants given by the VTST-ISPE procedure with corrections at four or five nonstationary points at the same electronic level. Our results showed, in agreement with Chuang *et al.*,[51b] that the best strategy consists first in putting two points very close to the saddle point ($s=-0.051$ bohr, $+0.051$ bohr). Having made this choice, the best location for adding two more points appears to be close to the turning points for the tunneling calculation at the representative tunneling energy for the lowest temperature of interest. In our study the turning points corresponding to the representative tunneling energy at 200 K are $s=-0.845$ bohr and $s=+0.029$ bohr and the extra single-point energy calculations were done at $s=-0.900$ bohr and $s=+0.031$ bohr. We added a fifth extra single-point energy calculated at $s=-0.200$ bohr, which is the location of the variational transition state at 0 K in the CCSD(T)//MP2/cc-pVTZ calculation with the 35 single-point energy set. The CVT/SCT rate constants obtained using the VTST-ISPE methodology and the five single-point energy corrections just described are given in the fourth column of Table III. The CVT/SCT rate constants calculated with the VTST-ISPE algorithm only differ from the CCSD(T)//MP2/cc-pVTZ/// rate constants based on a dense set of 35 nonstationary points by a factor of 1.04 at 200 K and a factor of 1.00 at 1500 K. Those figures confirm that there is no systematic advantage in adding single-point energies all along the reaction path and that one should use the resulting savings of resources to raise the level of electronic structure theory.

In Table IV the CVT/SCT rate constants for (R1) to (R6) at the CCSD(T)/aug-cc-pVTZ//MP2/cc-pVTZ level are given. These rate constants are calculated with the VTST-ISPE-5 ($s=-0.900$, $-0.200$, $-0.051$, $+0.031$, $+0.051$ bohr) single-point energy approach. The CVT/SCT rate constants values for (R1) show a significant increase (within a factor of 7 at 200 K and within a factor of 1.3 at 1500 K) when compared to the same rate constants for (R1) at the CCSD(T)//MP2/cc-pVTZ/// level (in Table III). The

TABLE IV. Rate constants (in $cm^3\,molecule^{-1}\,s^{-1}$) at several temperatures (power of 10 in parentheses) for (R1)–(R6) using VTST-ISPE algorithm at the CCSD(T)/aug-cc-pVTZ//MP2/cc-pVTZ level.

| $T$(K) | (R1) | (R2) | (R3) | (R4) | (R5) | (R6) |
|---|---|---|---|---|---|---|
| 200 | 4.83(−17) | 3.43(−17) | 2.42(−17) | 1.58(−17) | 1.12(−17) | 7.16(−17) |
| 223 | 1.30(−16) | 9.52(−17) | 6.97(−17) | 4.75(−17) | 3.43(−17) | 1.84(−16) |
| 298 | 1.40(−15) | 1.14(−15) | 8.79(−16) | 6.78(−16) | 5.35(−16) | 1.79(−15) |
| 300 | 1.47(−15) | 1.20(−15) | 9.28(−16) | 7.18(−16) | 5.67(−16) | 1.88(−15) |
| 350 | 4.58(−15) | 3.57(−15) | 3.05(−15) | 2.45(−15) | 2.00(−15) | 5.41(−15) |
| 400 | 1.07(−14) | 8.98(−15) | 7.79(−15) | 6.47(−15) | 5.43(−15) | 1.30(−14) |
| 420 | 1.47(−14) | 1.24(−14) | 1.08(−14) | 9.04(−15) | 7.65(−15) | 1.75(−14) |
| 500 | 4.16(−14) | 3.58(−14) | 3.11(−14) | 2.76(−14) | 2.40(−14) | 4.85(−14) |
| 600 | 1.11(−13) | 9.77(−14) | 8.50(−14) | 7.51(−14) | 7.02(−14) | 1.27(−13) |
| 700 | 2.38(−13) | 2.12(−13) | 1.84(−13) | 1.67(−13) | 1.60(−13) | 2.69(−13) |
| 1000 | 1.13(−12) | 1.02(−12) | 9.22(−13) | 8.64(−13) | 8.48(−13) | 1.25(−12) |
| 1500 | 4.77(−12) | 4.46(−12) | 4.26(−12) | 4.12(−12) | 4.17(−12) | 5.34(−12) |

CCSD(T)/aug-cc-pVTZ//MP2/cc-pVTZ rate constants are also higher than the MP-SAC2//MP2/adj-cc-pVTZ/// results except at 1500 K (see Table III). However, in comparison with experiment, the CVT/SCT rate constants for (R1) with our highest single-point energy level are still underestimating the experimental results for the whole range of temperatures. In Figs. 3(a)–3(f) we have plotted the theoretical Arrhenius plots for the six abstraction reactions along with the experimental results. It can be observed that the calculated rate constants are lower than the experimental values for the per-

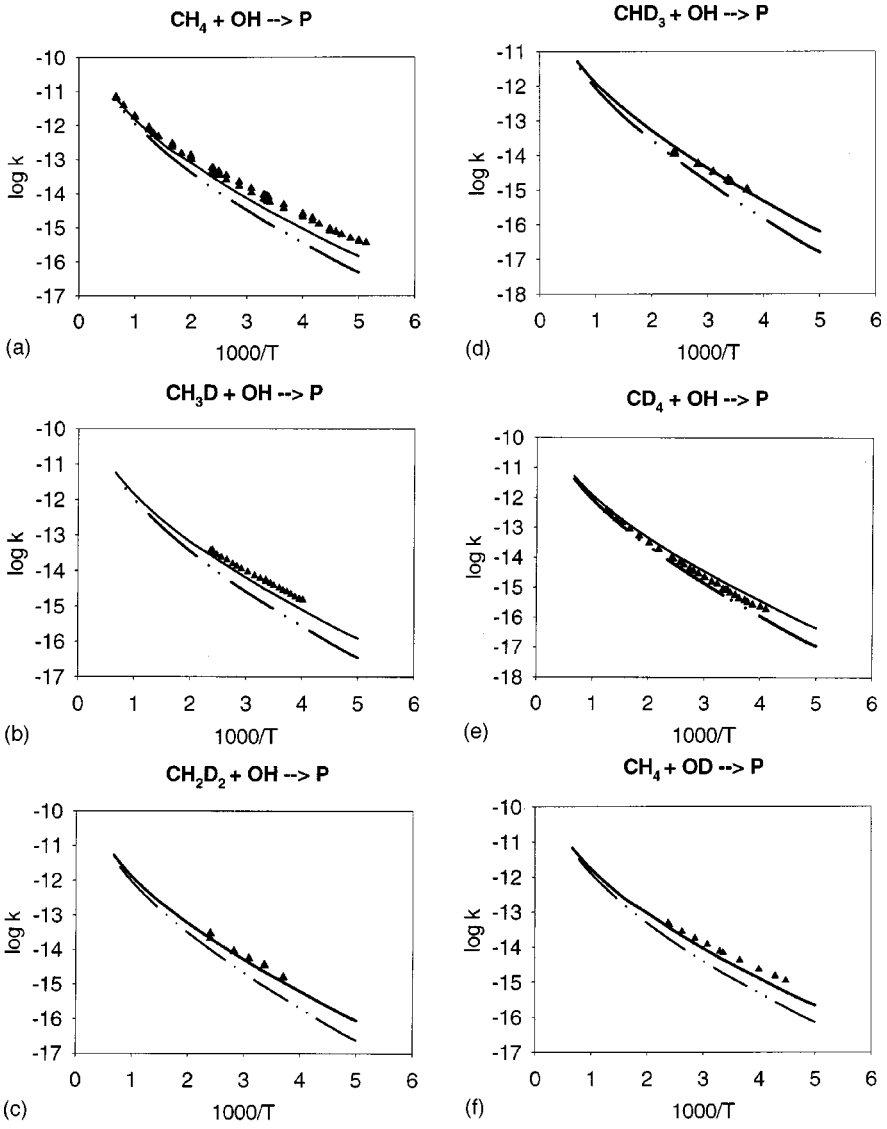


FIG. 3. Arrhenius plots for the experimental and calculated rate constants of: (a) (R1); (b) (R2); (c) (R3); (d) (R4); (e) (R5); and (f) (R6). Rate constants are in $cm^3\,molecule^{-1}\,s^{-1}$ and temperatures in Kelvin. Experimental data from Refs. 5–12 (triangles); CCSD(T)/aug-cc-pVTZ//MP2/cc-pVTZ level (dash-dot-dot line); CCSD(T)-SAC//MP2/cc-pVTZ level (solid line).

TABLE V. Rate constants (in $cm^3\,molecule^{-1}\,s^{-1}$) at several temperatures (power of 10 in parentheses) for (R1)–(R6) using VTST-ISPE algorithm at the CCSD(T)-SAC//MP2/cc-pVTZ level.

| $T$(K) | (R1) | (R2) | (R3) | (R4) | (R5) | (R6) |
|---|---|---|---|---|---|---|
| 200 | 1.45(−16) | 1.23(−16) | 9.13(−17) | 6.30(−17) | 4.48(−17) | 2.16(−16) |
| 223 | 3.60(−16) | 3.09(−16) | 2.36(−16) | 1.72(−16) | 1.27(−16) | 5.13(−16) |
| 298 | 3.33(−15) | 2.92(−15) | 2.34(−15) | 1.88(−15) | 1.51(−15) | 4.32(−15) |
| 300 | 3.50(−15) | 3.07(−15) | 2.46(−15) | 1.98(−15) | 1.59(−15) | 4.52(−15) |
| 350 | 9.96(−15) | 8.80(−15) | 7.13(−15) | 5.81(−15) | 4.92(−15) | 1.24(−14) |
| 400 | 2.29(−14) | 2.03(−14) | 1.67(−14) | 1.39(−14) | 1.17(−14) | 2.78(−14) |
| 420 | 3.06(−14) | 2.72(−14) | 2.24(−14) | 1.88(−14) | 1.59(−14) | 3.68(−14) |
| 500 | 8.06(−14) | 6.53(−14) | 5.88(−14) | 5.16(−14) | 4.49(−14) | 9.45(−14) |
| 600 | 1.77(−13) | 1.63(−13) | 1.48(−13) | 1.34(−13) | 1.19(−13) | 2.02(−13) |
| 700 | 3.57(−13) | 3.31(−13) | 2.94(−13) | 2.80(−13) | 2.54(−13) | 4.03(−13) |
| 1000 | 1.51(−12) | 1.42(−12) | 1.29(−12) | 1.20(−12) | 1.19(−12) | 1.68(−12) |
| 1500 | 6.23(−12) | 5.65(−12) | 5.49(−12) | 5.19(−12) | 5.25(−12) | 6.65(−12) |

protio reaction [(R1)] as well as for the five isotopic variants [reactions (R2) to (R6)]. However, the agreement improves if we increase the deuterium isotope composition of the methane reactant molecule, that is from $CH_4$ [(R1)] to $CD_4$ [(R5)]. The theoretical rate constants for the abstraction reaction by OD [(R6)] are also underestimated in comparison to experimental measurements.

The results presented so far demonstrate that the single-point energy corrections at the CCSD(T)/cc-pVTZ and at the CCSD(T)/aug-cc-pVTZ level may not be describing properly the PES for the abstraction reactions studied in this work. The problem arises from the use of an incomplete basis set, on one hand, and from the partial introduction of correlation energy at the CCSD(T) level. In addition, the CCSD(T)/cc-pVTZ and CCSD(T)/aug-cc-pVTZ electronic structure calculations may suffer form the lack of correlation balance that it is needed to account, on equal grounds, for the cleavage of a C–H bond and the formation of a O–H bond. The SAC procedure of Truhlar and co-workers[14] was developed for extrapolating correlated electronic structure calculations to the limit of full dynamical correlation and complete one-electron basis sets. In the MP-SAC2//MP2/adj-cc-pVTZ calculations,[15a] the scaling factor ($F$) was specifically parametrized for the perprotio reaction and the cc-pVTZ basis set was adjusted to achieve the correlation balance between the C–H and O–H bonds. We have seen that the dynamical results with single-point energy corrections at the MP-SAC2//MP2/adj-cc-pVTZ level are in better agreement with experiment than rate constants calculated with single-point energy corrections at the CCSD(T)//MP2/cc-pVTZ level. For this reason we decided also to test the recently developed CCSD(T)-SAC/cc-pVTZ parametrization of Truhlar and co-workers[35] for the calculation of rate constants. In the CCSD(T)-SAC approach the optimum value for the $F$ parameter was found in a general way by minimizing the root-mean-square deviation of the calculated atomization energies for a set of molecules from the experimental values. It was assessed in the same paper that the resulting $F$ parameter should be more widely useful for calculating barrier heights for chemical reactions.

The CVT/SCT rate constants calculated at the CCSD(T)-SAC//MP2/cc-pVTZ level using the VTST-ISPE-5 ($s=-0.900$, $-0.200$, $-0.051$, $+0.031$, $+0.051$ bohr) methodology are presented in Table V for (R1) to (R6) reactions. The corresponding Arrhenius plots are also given in Figs. 3(a)–3(f). In comparison with the previous dual-level dynamical results presented in this work, the rate constants using CCSD(T)-SAC high level for correcting the energies are higher and show the best agreement with experiment for (R1) and for the whole set of isotopic variants at all the temperatures studied. From the Arrhenius plots, it can be observed that the calculated CVT/SCT rate constants for (R1) underestimate the experimental results, especially at low temperatures. Conversely, the calculated (R5) rate constants turn out to be slightly overestimated. Since the reactions corresponding to $CH_3D$, $CH_2D_2$, and $CHD_3$ involve, as mentioned above, a progressive contribution of the C–D bond breaking, the agreement with the experimental results becomes gradually better in going from (R2) to (R4). The theoretical rate constants for (R6) are also slightly underestimated. In Fig. 4 we have plotted the adiabatic profiles for (R1) and (R5) calculated at the CCSD(T)-SAC//MP2/cc-pVTZ and CCSD(T)/aug-cc-pVTZ//MP2/cc-pVTZ levels. One can see that the SAC correction lowers the adiabatic barrier and makes it thinner. The adiabatic barrier height at the CCSD(T)/aug-cc-pVTZ//MP2/cc-pVTZ and CCSD(T)-SAC//MP2/cc-pVTZ levels is 6.2 kcal/mol ($s=-0.291$ bohr) and 5.6 kcal/mol ($s=-0.330$ bohr), respectively.

From the comparison of conventional transition-state (TST) rate constants with canonical variational transition state (CVT) values, it can be stated that variational effects are important for the whole set of abstraction reactions studied in this work. These variational effects are most significant for (R1) at low temperatures [at 200 K the CVT rate constant for (R1) is about two orders of magnitude smaller than the TST rate constant] and they gradually become smaller in going from (R1) to (R5) and in increasing temperature. At 1500 K the TST/CVT rate constants ratio for R5 is only of 1.10. For R6 the TST/CVT rate constants factors are 34.4 at 200 K and 1.8 at 1500 K.

On the other hand, the comparison of the CVT and CVT/SCT rate constants have shown that multidimensional tunneling corrections must be included in the computation of the rate coefficients for the abstraction reactions (R1) to (R5). At 200 K the SCT transmission coefficient at CCSD(T)-SAC//

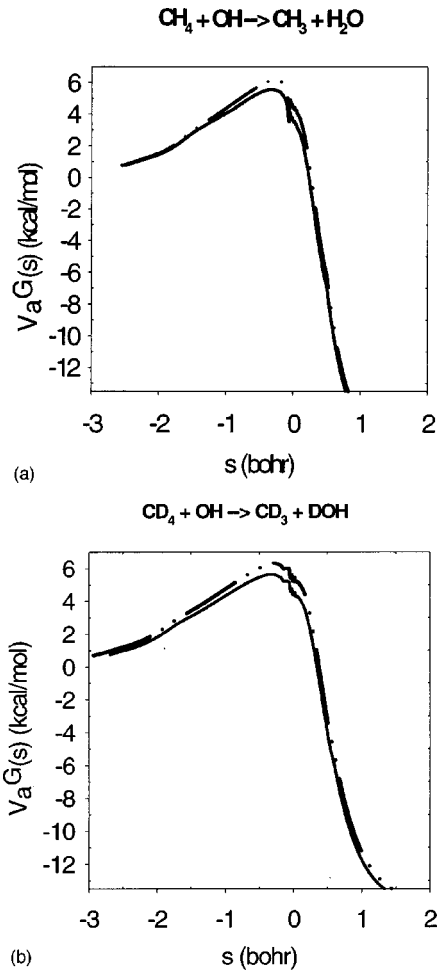


FIG. 4. Adiabatic potential energy curve ($V_a^G$) as a function of $s$ for (a) (R1); and (b) (R5), at the CCSD(T)/aug-cc-pVTZ//MP2/cc-pVTZ level (dash-dot-dot line), and at the CCSD(T)-SAC//MP2/cc-pVTZ level (solid line). All vibrational frequencies are scaled by 0.9790.

MP2/cc-pVTZ level increases the CVT rate constant by 8.6 and by 6.0 for (R1) and (R5), respectively, and by 7.91 for (R6). The correction for tunneling only becomes nearly 1.0 at the highest temperatures studied.

## IV. CONCLUSIONS

Previous results from other authors on the dynamics of the reactions $CH_4D_{4-n}+OH\rightarrow P$, together with our own results, have shown that an accurate description of the rate constants of these abstraction reactions is still an authentic challenge for current computational methods. Our results also demonstrate that variational effects and tunneling corrections have to be included in the calculation of the rate constants of these reactions. Consequently, conventional transition-state theory should not be used and a monodimensional approach to tunneling might not be accurate enough. We have carried out canonical variational transition state theory plus multidimensional tunneling (CVT/MT) direct dynamics calculations at the CCSD(T)/aug-cc-pVTZ//MP2/cc-pVTZ and CCSD(T)-SAC//MP2/cc-pVTZ levels, which correspond to the present state of the art of the monoreference electronic structure methods. Even so, and although our results are quite good, we still do not match exactly the last available experimental rate constants. The degree of deviation of our theoretical CVT/MT rate constants from experimental results as a function of temperature probably indicates that the maximum of the adiabatic profile of 6.2 and 5.6 kcal/mol at the CCSD(T)/aug-cc-pVTZ//MP2/cc-pVTZ and CCSD(T)-SAC//MP2/cc-pVTZ levels, respectively, is quite accurate for the perprotio reaction. The main pitfalls of the electronic structure calculations (energies, gradients, and frequencies) can come from the description of the adiabatic profile in that region away from the transition-state location which is still crucial for tunneling corrections. Additional theoretical work on these reactions, including multicoefficient methods[64] or multireference methods, is now in progress in our laboratory.

## ACKNOWLEDGMENTS

We thank DGESIC for financial support through project No. PB98-0915. The use of the computational facilities of the CESCA and CEPBA coordinated by the $C^4$ is gratefully acknowledged.

[1] J. Warnatz, in *Combustion Chemistry*, edited by W. C. Gardiner, Jr. (Springer, New York, 1984), p. 28.
[2] B. J. Finlayson-Pitts and J. N. Pitts, Jr., in *Atmospheric Chemistry* (Wiley, New York, 1986).
[3] R. Atkinson, Chem. Rev. **86**, 69 (1986), and references therein.
[4] J. F. Comes, Angew. Chem. Int. Ed. Engl. **33**, 1816 (1994).
[5] S. Gordon and W. A. Mulac, Int. J. Chem. Kinet. **1**, 289 (1975).
[6] D. L. Baulch, M. Bowers, D. G. Malcom, and R. T. Tuckerman, J. Phys. Chem. Ref. Data **15**, 465 (1986), and references therein.
[7] R. Atkinson, J. Phys. Chem. Ref. Data **1**, 18 (1989).
[8] G. L. Vaghjiani and A. R. Ravishankara, Nature (London) **350**, 406 (1991).
[9] J. R. Dunlop and F. P. Tully, J. Phys. Chem. **97**, 11148 (1993).
[10] W. B. DeMore, J. Phys. Chem. **97**, 8564 (1993).
[11] W. B. DeMore, S. P. Sander, D. M. Golden *et al.* ''Chemical kinetics and photochemical data for use in stratospheric modeling,'' Jet Propulsion Laboratory (1994).
[12] T. Gierczak, R. K. Talukdar, S. C. Herndon, G. L. Vaghjiani, and A. R. Ravishankara, J. Phys. Chem. A **101**, 3125 (1997).
[13] T. N. Truong and D. G. Truhlar, J. Chem. Phys. **93**, 1761 (1990).
[14] M. S. Gordon and D. G. Truhlar, J. Am. Chem. Soc. **108**, 5412 (1986).
[15] (a) V. S. Melissas and D. G. Truhlar, J. Chem. Phys. **99**, 1013 (1993); (b) V. S. Melissas and D. G. Truhlar *ibid.* **99**, 3542 (1993).
[16] A. González-Lafont, T. N. Truong, and D. G. Truhlar, J. Chem. Phys. **95**, 8875 (1991).
[17] Y.-P. Liu, G. C. Lynch, T. N. Truong, D.-h. Lu, D. G. Truhlar, and B. C. Garrett, J. Am. Chem. Soc. **115**, 2408 (1993).
[18] W.-P. Hu, Y.-P. Liu, and D.-G. Truhlar, J. Chem. Soc., Faraday Trans. **90**, 1715 (1994).
[19] (a) Y.-P. Liu, D.-h. Lu, A. González-Lafont, D. G. Truhlar, and B. C. Garrett, J. Am. Chem. Soc. **115**, 7806 (1993); (b) D. G. Truhlar, J. Chem. Soc., Faraday Trans. **90**, 1740 (1994).
[20] A. González-Lafont, T. N. Truong, and D. G. Truhlar, J. Phys. Chem. **95**, 4618 (1991).
[21] K. D. Dobbs, D. A. Dixon, and A. Komornicki, J. Chem. Phys. **98**, 8852 (1993).
[22] M. Schwartz, P. Marshall, R. J. Berry, C. J. Ehlers, and G. A. Petersson, J. Phys. Chem. A **102**, 10074 (1998).
[23] J. Korchowiec, S. Kawahara, K. Matsumura, T. Uchimaru, and M. Sugie, J. Phys. Chem. A **103**, 3548 (1999).
[24] J. Espinosa-García and J. C. Corchado, J. Chem. Phys. **112**, 5731 (2000).
[25] D. G. Truhlar, A. D. Isaacson, and B. C. Garrett, in *Theory of Chemical Reaction Dynamics*, edited by M. Baer (CRC, Boca Raton, 1985), Vol. IV, p. 65.
[26] S. C. Tucker and D. G. Truhlar, in *New Theoretical Concepts for Understanding Organic Reactions*, edited by J. Bertrán and I. G. Csizmadia (Kluwer Academic, Dordrecht, 1989), p. 291.

[27] GAUSSIAN94, M. J. Frisch, G. W. Trucks, H. B. Schlegel *et al.* (Gaussian, Inc., Pittsburgh, PA, 1995).
[28] POLYRATE8.2, Y.-Y. Chuang, J. C. Corchado, P. L. Fast *et al.*, University of Minnesota, Minneapolis, 1999.
[29] W. J. Hehre, L. Radom, P. v. R. Schleyer, and J. A. Pople, in *Ab Initio Molecular Orbital Theory* (Wiley, New York, 1986).
[30] C. Møller and M. S. Plesset, Phys. Rev. **46**, 618 (1934).
[31] T. H. Dunning, Jr., J. Chem. Phys. **90**, 1007 (1989).
[32] K. Raghavachari, G. W. Trucks, J. A. Pople, and M. Head-Gordon, Chem. Phys. Lett. **157**, 479 (1989).
[33] D. E. Woon and T. H. Dunning, Jr., J. Chem. Phys. **98**, 1358 (1993).
[34] R. A. Kendall, T. H. Dunning, Jr., and R. J. Harrison, J. Chem. Phys. **96**, 6796 (1992).
[35] P. L. Fast, J. C. Corchado, M. L. Sánchez, and D. G. Truhlar, J. Phys. Chem. A **103**, 3139 (1999).
[36] (a) D. G. Truhlar and A. Kupperman, J. Am. Chem. Soc. **93**, 1840 (1971); (b) K. Fukui, Pure Appl. Chem. **54**, 1825 (1982).
[37] C. Gonzalez and H. B. Schlegel, J. Phys. Chem. **94**, 5523 (1990).
[38] B. C. Garrett and D. G. Truhlar, J. Chem. Phys. **70**, 1593 (1979).
[39] A. D. Isaacson and D. G. Truhlar, J. Chem. Phys. **76**, 1380 (1982).
[40] B. C. Garrett and D. G. Truhlar, J. Phys. Chem. **83**, 1079 (1979).
[41] B. C. Garrett, D. G. Truhlar, R. S. Grev, and A. W. Magnuson, J. Phys. Chem. **84**, 1730 (1980).
[42] B. C. Garrett and D. G. Truhlar, J. Am. Chem. Soc. **101**, 4534 (1979).
[43] B. C. Garrett and D. G. Truhlar, J. Am. Chem. Soc. **101**, 5207 (1979).
[44] P. Pechukas, J. Chem. Phys. **64**, 1516 (1976).
[45] J. Villà and D. G. Truhlar, Theor. Chem. Acc. **97**, 317 (1997).
[46] Y.-Y. Chuang and D. G. Truhlar, J. Phys. Chem. A **102**, 242 (1998).
[47] A. P. Scott and L. Radom, J. Phys. Chem. **100**, 16502 (1996).
[48] Y.-Y. Chuang and D. G. Truhlar, J. Chem. Phys. **112**, 1221 (2000).
[49] J. E. Kilpatrick and K. S. Pitzer, J. Chem. Phys. **17**, 1064 (1949).
[50] J. C. Corchado, E. L. Coitiño, Y.-Y. Chuang, P. L. Fast, and D. G. Truhlar, J. Phys. Chem. A **102**, 2424 (1998).
[51] (a) W. T. Duncan, R. L. Bell, and T. N. Truong, J. Comput. Chem. **19**, 1039 (1998). (b) Y.-Y. Chuang, J. C. Corchado, and D. G. Truhlar, J. Phys. Chem. A **103**, 1140 (1999).
[52] W.-P. Hu and D. G. Truhlar, J. Am. Chem. Soc. **118**, 860 (1996).
[53] H. Basch and S. Hoz, J. Phys. Chem. A **101**, 4416 (1997).
[54] M. D. Wheeler, M. Tsiouris, M. I. Lester, and G. Lendvay, J. Chem. Phys. **112**, 6590 (2000).
[55] L. Masgrau, A. González-Lafont, and J. M. Lluch, J. Phys. Chem. A **103**, 1044 (1999).
[56] B. J. Lynch, P. L. Fast, M. Harris, and D. G. Truhlar, J. Phys. Chem. A **104**, 4811 (2000).
[57] Y.-Y. Chuang, E. L. Coitiño, and D. G. Truhlar, J. Phys. Chem. A **104**, 446 (2000).
[58] D. A. Dixon and D. Feller, J. Phys. Chem. A **102**, 8209 (1998).
[59] D. K. Malick, G. A. Petersson, and J. A. Montgomery, Jr., J. Chem. Phys. **108**, 5704 (1998).
[60] D. J. Tozer and N. C. Handy, J. Phys. Chem. A **102**, 3162 (1998).
[61] F. A. Hamprecht, A. J. Cohen, D. J. Tozer, and N. C. Handy, J. Chem. Phys. **109**, 6264 (1998).
[62] M. Sodupe, J. Bertrán, L. Rodríguez-Santiago, and E. J. Baerends, J. Phys. Chem. A **103**, 166 (1999).
[63] O. Roberto-Nieto, F. B. C. Machado, and D. G. Truhlar, J. Chem. Phys. **111**, 10046 (1999).
[64] P. L. Fast, J. C. Corchado, M. L. Sánchez, and D. G. Truhlar, J. Phys. Chem. A **103**, 5129 (1999).